The Diverse Origins of Terrestrial-Planet Systems

Makiko Nagasawa
National Astronomical Observatory of Japan

Edward W. Thommes
Canadian Institute for Theoretical Astrophysics

Scott J. Kenyon
Smithsonian Astrophysical Observatory

Benjamin C. Bromley
University of Utah

Douglas N. C. Lin
University of California, Santa Cruz

We review the theory of terrestrial planet formation as it currently stands. In anticipation of forthcoming observational capabilities, the central theoretical issues to be addressed are: 1) what is the frequency of terrestrial planets around nearby stars, 2) what mechanisms determine the mass distribution, dynamical structure and the stability of terrestrial-planet systems, and 3) what processes regulated the chronological sequence of gas and terrestrial planet formation in the Solar System? In the context of Solar System formation, the last stage of terrestrial planet formation will be discussed along with cosmochemical constraints and different dynamical architectures together with important processes such as runaway and oligarchic growth. Observations of dust around other stars, combined with models of dust production during accretion, give us a window on exo-terrestrial planet formation. We discuss the latest results from such models, including predictions which will be tested by next-generation instruments such as GMT and ALMA.

1. INTRODUCTION

Our home in the Solar System: Third planet, 150 million km from the Sun, 70 percent ocean, possessing a large moon and a moderate climate. How was it born, and how did it grow? How ubiquitous are planets like it in the universe? Such questions have been asked throughout human history. Recent advances in both theory and observation have brought us closer to the answers.

Following the first discovery of an extrasolar planet around 51 Peg, more than 150 planets have been announced, including such fascinating specimens as the multi-planet system of Upsilon Andromeda, and the Neptune-mass planet in 55 Cnc (e.g., *Mayor and Queloz*, 1995; *Butler et al.*, 1999; *McArthur et al.*, 2004). In just ten years, observational techniques have come to within an order of magnitude of being able to find an Earth-mass planet. The detected extrasolar planets turned on their head the standard models of planetary formation (e.g., *Safronov*, 1969; *Hayashi et al.*, 1985) which were proposed in the 1970s. The seemingly sensible architecture of our Solar System, with four terrestrial planets orbiting inside 2AU, plus gas and icy planets orbiting outside the "snow line", all on reassuringly circular orbits, turned out to be far from the only possible configuration. On the contrary, short orbital periods, high eccentricities and large planetary masses have made for a diversity of planetary systems unimagined a decade ago (*Marcy et al.*, 2004; *Mayor et al.*, 2004). The theory of planet formation has likewise made rapid progress, helped by these observations and by increases in computing power. We can now numerically simulate many aspects of the formation process in great detail. Thus we have moved well beyond the dawn of planetary science, into an era of fast-paced development. It is thus an exciting time to review the current state of the theory of terrestrial planet formation.

2. BACKGROUND

In the standard scenario, terrestrial planets form through 1) dust aggregation and settling in the protoplanetary disk, 2) planetesimal formation from grains in a thin midplane, 3) protoplanet accretion from planetesimals, and 4) final accumulation by giant impacts. Here, we begin with

an overview of the first stages and then focus on chaotic growth, the last stage of terrestrial planetary formation.

Although analytic studies are the foundation for this picture, numerical calculations are essential to derive the physical properties of planetary systems. There are two broad classes of simulations. The statistical approach (*Wetherill and Stewart*, 1989, 1993) can follow collisional growth – including collisional disruption and evolution of dust grains – over long times with modest computational effort (*Inaba et al.*, 2001, and references therein). This approach works best for the first three stages, where statistical approximations are accurate and large-scale dynamical interactions are small. Direct N-body calculations (*Kokubo et al.*, 1998; *Chambers*, 2001) are computationally expensive but can follow key dynamical phenomena such as resonant interactions important during the final stages of planet growth. All calculation benefit from advances in computing power. In particular, N-body simulations no longer require an artificial scaling parameter to speed up the evolution and are thus more reliable (*Kokubo and Ida* 2000).

2.1. From Dust to Planetesimals

The growth of km-sized planetesimals involves complex interactions between dust and gas within the protoplanetary disk (e.g., *Dominik et al.*, this volume; *Weidenschilling and Cuzzi*, 1993; *Ward*, 2000). The vertical component of the star's gravity pulls mm-sized and larger grains toward the midplane, where they settle into a thin disk. Smaller grains are more strongly coupled to turbulence in the gas and remain suspended above the midplane. The gas disk is partly pressure-supported and rotates at slightly less than Keplerian velocity. The dust grains thus feel a headwind and undergo orbital decay by aero-drag. The drag is strongest for m-size particles (e.g., *Adachi et al.*, 1976; *Tanaka and Ida*, 1999), which fall into the star from 1 AU in $\sim$ 100 yr. It is not yet clear whether m-sized objects have enough time to grow directly to km-sized planetesimals which are safe from gas drag (*Dominik et al.*, this volume).

Dynamical instability mechanisms sidestep the difficulties of direct accumulation of planetesimals (e.g., *Goldreich and Ward*, 1973; *Youdin and Shu*, 2002). If the turbulence in the gas is small, the dusty midplane becomes thinner and thinner until groups of particles overcome the local Jeans criterion – where their self-gravity overcomes tidal forces from the central star – and 'collapse' into larger objects. Although this gravitational instability is promising, it is still uncertain whether the turbulence in the disk is large enough to prevent the instability (*Weidenschiling and Cuzzi*, 1993; *Weidenschiling*, 1995). The range of planetesimal sizes produced by the instability is also uncertain.

2.2. From Planetesimals to Protoplanets

Once planetesimals reach km sizes, they begin to interact gravitationally. Collisions produce mergers and tend to circularize the orbits. Long range gravitational interactions exchange kinetic energy (dynamical friction) and angular momentum (viscous stirring), redistributing orbital energy among planetesimals. Gas drag damps the orbits of planetesimals. For planetesimals without an external perturber, the collisional cross-section is

$$\sigma = \pi d^2 f_{\rm g} = \pi d^2 \left(1 + \frac{v_{\rm esc}^2}{v^2}\right), \qquad (1)$$

where d is the radius of a particle with mass m, v is its velocity relative to a Keplerian orbit, and $v_{\rm esc}^2 = 2Gm/d$ is the escape velocity (*Wetherill*, 1990; *Ohtsuki et al.*, 1993; *Kortenkamp et al.*, 2000). With no outside perturbations, $v \approx v_{\rm esc}$, and gravitational focusing factors, $f_{\rm g} \sim 1$, are small. Thus, growth is slow and orderly (*Safronov*, 1969).

During orderly growth, long range gravitational interactions between growing planetesimals become important. Small particles damp the orbits of larger particles; larger particles stir up the orbits of smaller particles (*Wetherill and Stewart*, 1993; *Kokubo and Ida*, 1995). In cases where gas drag is negligible compared to viscous stirring, the relative orbital velocities of the largest ('l') and smallest ('s') bodies reach an approximate steady-state with

$$\frac{v_l}{v_s} = \left(\frac{\Sigma_l}{\Sigma_s}\right)^n, \qquad (2)$$

where $n \approx$ 1/4 to 1/2 and Σ is the surface density (*Kokubo and Ida*, 1996; *Goldreich et al.*, 2004). When planetesimals are small, $\Sigma_l/\Sigma_s \ll 1$ and $v_l/v_s < 1$. As planetesimals grow, their escape velocity also grows, which leads to $f_{\rm g} \gg 1$ and the onset of runaway growth.

Runaway growth depends on a positive feedback between dynamical friction and gravitational focusing. Dynamical friction produces a velocity distribution that declines roughly monotonically with increasing mass (eq. 2). Although gas drag damps the orbits of these objects and keeps their velocities less than $v_{\rm esc}$, dynamical friction and viscous stirring maintain the small velocities of the largest objects. Because they have the largest $v_{\rm esc}$ and the smallest v, the largest objects have the largest gravitational cross-sections and the largest growth rates (eq. 1). Thus, a few large objects grow fastest and "run away" from the ensemble of planetesimals (*Wetherill and Stewart*, 1989, 1993; *Kokubo and Ida*, 1996).

Runaway growth also depends on a broad size distribution. For planetesimals with masses, m_1 and m_2, and relative velocities, v_1 and v_2, stirring from dynamical friction is $\sim (m_1 v_1^2 - m_2 v_2^2)$. With $v_1 \approx v_2$ initially, dynamical friction becomes important when $m_2 \gtrsim 10 m_1$. For planetesimals at 1 AU, dynamical friction dominates the evolution when $m_2 \sim (10^4 - 10^6) m_1 \sim 10^{20}$–$10^{24}$ g for planetesimals with radii of 1–10 km ($m_1 \sim 10^{16}$–10^{19} g; *Ohtsuki et al.*, 1993). The typical timescale for planetesimals to reach $m_2 \sim 10^{24}$ g is $\sim 10^4$–10^5 yr at 1 AU (*Wetherill and Stewart*, 1989, 1993; *Weidenschilling et al.*, 1997).

As a few protoplanets contain an ever increasing fraction of the total mass, two processes halt runaway growth (*Ida and Makino*, 1993; *Kokubo and Ida*, 1998). Proto-

planets stir up leftover planetesimals, reducing their gravitational cross-sections. With less mass in planetesimals, dynamical friction between the smallest planetesimals and the largest protoplanets cannot maintain the low velocities of the largest objects, reducing gravitational cross-sections further (eq.1, 2). Because the largest protoplanet stirs up its surroundings the most, its growth slows down the most, allowing smaller protoplanets to catch up before their growth rates also slow down. This process results in an "oligarchy" of (locally) similar-mass protoplanets (*Kokubo and Ida* 1998). Protoplanets reach oligarchy faster closest to the central star, where the surface density of dust is largest and the orbital period is shortest. Thus, the onset of oligarchy sweeps from the inside to the outside of the disk. Although smaller "oligarchs" grow faster than larger ones, oligarchs continue to sweep up leftover planetesimals and thus contain a larger and larger fraction of the total mass in the disk.

During oligarchic growth, protoplanets isolate themselves from their neighbors. Mutual gravitational interactions push them apart to maintain relative separations of $\sim$ 10 Hill radii ($r_{\rm H}$; *Kokubo and Ida*, 1995, 1998). Dynamical friction circularizes their orbits. The large orbital separations and circular orbits yield a maximum "isolation mass," derived from the mass of planetesimals within the $\sim 10 r_{\rm H}$ annulus, $\sim$ 0.1–0.2 $M_\oplus$, roughly 10%–20% of an Earth mass (see below). The typical timescale to reach this isolation mass is $\sim 10^5$–10^6 yr (*Kokubo and Ida*, 1998).

2.3. From Protoplanets to Planets

With isolation masses a small fraction of the mass of the Earth or Venus, dynamical interactions among the oligarchs must become more energetic to complete terrestrial planet formation. When oligarchs have accumulated most of the planetesimals in their isolation zones, dynamical friction between planetesimals and oligarchs cannot balance dynamical interactions among the oligarchs. Oligarchy ends. Chaotic growth, where planets grow by giant impacts and continued accretion of small planetesimals, begins.

The transition from oligarchy to chaos depends on the balance between damping and dynamical interactions. With no external perturber – a massive planet or a binary companion – the transition occurs when the surface density in oligarchs roughly equals the surface density in planetesimals (*Goldreich et al.*, 2004; *Kenyon and Bromley*, 2006). The transition occurs in $\sim$ 10 Myr (e.g., *Chambers et al.*, 1996). Dynamical perturbations by a Jovian planet or a binary companion shorten this timescale (*Ito and Tanikawa*, 1999); damping processes lengthen it (*Iwasaki et al.* 2001, 2002). Once isolation is overcome, protoplanets grow to planets in $\sim$ 10–300 Myr (e.g., *Chambers and Wetherill*, 1998; *Chambers*, 2001; *Kenyon and Bromley*, 2006).

2.4. Outcomes of Numerical Simulations

Attempts to simulate the assembly of terrestrial planets using statistical and N-body approaches began in the late 1970's (*Greenberg et al.*, 1978). Although statistical methods have evolved from single annulus (*Wetherill and Stewart*, 1993) to multiannulus techniques (*Weidenschilling et al.*, 1997), the main result is robust: all calculations yield 10–40 isolated Mars-sized protoplanets in roughly circular orbits and many leftover planetesimals on highly eccentric orbits. During oligarchic growth, fragmentation of the leftovers introduces uncertainties in the timescales and outcomes, as described in Section 3 and Section 4.

With tens to a few hundred protoplanets remaining at the end of oligarchic growth, direct N-body simulations provide the only way to follow the orbital interactions over hundreds of Myr. Indeed, the first direct N-body (*Cox and Lewis*, 1980; *Lecar and Aarseth*, 1986) and Monte-Carlo Öpik-Arnold scheme simulations (e.g., *Wetherill*, 1985, 1996), demonstrate that collisions of Moon-sized objects yield "solar systems" containing at least one planet with $m \gtrsim M_\oplus/3$ at $\sim$ 1 AU around a solar-mass star. However, these simulations also show that the outcomes are stochastic and sensitive to the initial number and orbit distributions of the oligarchs. Thus, each set of initial conditions requires many realizations to derive statistically meaningful results.

Several groups have performed full N-body simulations of chaotic growth with and without dynamical influence from Jovian planets (e.g., *Chambers and Wetherill*, 1998; *Agnor et al.*, 1999; *Chambers*, 2001; *Kominami and Ida*, 2002, 2004; *Kokubo et al.*, 2006a). The simulations start with $\sim$ 20–200 oligarchs in circular or modestly elliptical orbits, with a radial surface density that declines with semimajor axis. Multiple runs ($\sim$ 10–200) having identical initial conditions except for, typically, random variations in orbital phase, provide a first measure of the repeatability of the results. These calculations yield similar results for the masses, spin angular momenta, and orbital properties of planets and leftover oligarchs. On timescales of 100–300 Myr, most simulations yield planets with (i) masses and semimajor axes similar to the terrestrial planets in the Solar System, (ii) orbital eccentricities and inclinations somewhat larger than those in the Solar System, and (iii) spins dominated by the last few giant impacts. Thus, planets similar to Earth and Venus are an inevitable outcome of chaotic growth. Mars appears to be a leftover oligarch.

In the context of these models, the circular orbits of the Earth and Venus in the Solar System require an additional damping mechanism. Dynamical friction (*Chambers* 2001) or gravitational drag by the remnant gas disk (e.g., *Ward* 1989, 1993; *Artymowicz* 1993; *Agnor and Ward* 2002) are good candidates. However, damping tends to prevent the orbital instability needed to initiate chaotic growth (*Iwasaki et al.* 2001, 2002). Other interactions with the gas, such as type I migration, tend to induce orbital decay in Mars-sized or larger planets (*Goldreich and Tremaine*, 1980; *Ward*, 1986; *McNeil et al. 2005*, *Papaloizou et al.*, this volume). These results suggest that the timescales for gas depletion and chaotic growth must be roughly comparable (Section 4.3; *Kominami and Ida*, 2002, 2004).

With this background set, we describe some useful analytic approximations for the runaway and oligarchic

growth phases (Section 3), review recent simulations of chaotic growth (Section 4), and then introduce the dynamical shake-up model (Section 4.3). We conclude with a final section describing the implications for future observing capabilities in Section 5.

3. EVOLUTION TO CHAOTIC GROWTH

Although numerical calculations are required to predict the time evolution of planetesimals and protoplanets, analytic derivations clarify basic physical processes and yield important estimates for the evolution of solid objects (*Lissauer*, 1987; *Lissauer and Stewart*, 1993; *Goldreich et al.*, 2004). These results also provide basic input for numerical calculations (*Ohtsuki*, et al. 1993, 2002). Here, we outline several results to introduce recent numerical simulations.

Most treatments of terrestrial planet formation begin with a prescription for the surface density Σ of gas and dust in the disk. The number, mass, and orbital separations of oligarchs depend on this prescription (*Kokubo and Ida*, 2002). Here, we adopt a disk with surface density

$$\Sigma_{\rm d} = \Sigma_{\rm d1}\left(\frac{a}{1{\rm AU}}\right)^{-\alpha} \quad {\rm dust}, \tag{3}$$

$$\Sigma_{\rm g} = \Sigma_{\rm g1}\left(\frac{a}{1{\rm AU}}\right)^{-\alpha} \quad {\rm gas}, \tag{4}$$

where a is the semimajor axis. In the Minimum Mass Solar Nebula (MMSN), $\alpha = 3/2$, $\Sigma_{\rm d1} \approx 7$ g cm^{-2}, and $\Sigma_{\rm g1} \approx 1700$ g cm^{-2} (*Hayashi et al.* 1985).

3.1. Some Analytic Estimates

To derive the growth rate, we start with eq. 1 and adopt subscripts 'f' for the field planetesimals, 'olig' for the oligarchs, and an asterisk ($*$) for the central star. The disk scale height is $h = v_{\rm f}/\Omega_{\rm kep}$, where $\Omega_{\rm kep} = (Gm_*/a^3)^{1/2}$ is the orbital frequency. For a mass density $\rho_{\rm d} = \Sigma_{\rm d}\Omega_{\rm kep}/v_{\rm f}$, the growth rate of particles is (e.g., *Wetherill*, 1980)

$$\frac{dm}{dt} \sim \pi d^2 \Sigma_{\rm d}(1 + (v_{\rm esc}/v_{\rm f})^2)\Omega_{\rm kep}. \tag{5}$$

The timescale for planetesimals to grow to an Earth mass is

$$t_{\rm grow} = \left(\frac{1}{m}\frac{dm}{dt}\right)^{-1} = 50\left(\frac{\Sigma_{\rm d1}}{10{\rm g\ cm^{-2}}}\right)^{-1}\left(\frac{\rho_{\rm m}}{3{\rm g\ cm^{-3}}}\right)^{2/3}\left(\frac{m_*}{M_\odot}\right)^{-1/2} \times \left(\frac{m}{M_\oplus}\right)^{1/3}\left(\frac{a}{1{\rm AU}}\right)^{3/2-\alpha}\left(1+\frac{v_{\rm esc}^2}{v_{\rm f}^2}\right)^{-1} {\rm Myr}, \tag{6}$$

where $\rho_{\rm m}$ is the bulk density of a planetesimal and $M_\odot$ is the mass of the Sun.

Initially, $v_{\rm f}$ is set by the balance of excitation from viscous stirring between field particles and damping due to gas drag. Adopting the drag force a spherical particle feels in the gas (e.g., *Adachi et al.*, 1976) and a gas density $\rho_{\rm g} \sim \Sigma_{\rm g}/2h$, the random velocity of a field particle is

$$v_{\rm f} \propto \Sigma_{\rm d}^{1/5}\left(\frac{\Sigma_{\rm g}}{h}\right)^{-1/5} m^{-1/15} v_{\rm esc,f} \equiv C v_{\rm esc,f} \tag{7}$$

where $C < 1$ (*Ida and Makino*, 1993).

When an oligarch grows among field planetesimals, $v_{\rm f} \equiv C' v_{\rm esc,olig}$ with $C' < 1$ ($v_{\rm f}$ is now set by the balance between viscous stirring due to the oligarchs and gas drag). In the runaway and oligarchic phases, respectively, the growth rates of particles are roughly

$$t_{\rm grow} \propto m^{1/3}\left[1 + \frac{1}{C^2}\left(\frac{m}{m_{\rm f}}\right)^{2/3}\right]^{-1}, \tag{8}$$

$$t_{\rm grow} \propto m^{1/3}\left[1 + \frac{1}{C'^2}\left(\frac{m}{m_{\rm olig}}\right)^{2/3}\right]^{-1}. \tag{9}$$

For particles with $m \gg m_{\rm f}$, $t_{\rm grow} \propto m^{-1/3}$ in the runaway stage. Larger bodies grow faster. Field plantesimals ($m = m_{\rm f}$ in eq. 8) have $t_{\rm grow,f} \propto m^{1/3}$ and undergo orderly growth (*Safronov*, 1969). When runaway growth ends, oligarchs ($m = m_{\rm olig}$ in eq. 9) and field planetesimals ($m/m_{\rm olig} \ll 1$) both formally undergo orderly growth, $t_{\rm grow} \propto m^{1/3}$. However, collisions among planetesimals cease to be accretional when $v_{\rm esc,olig} \gg v_{\rm esc,f}$. Thus, planetesimal growth is eventually inhibited during oligarchic growth (see Section 3.2 below).

Oligarchs have orbital separations $\Delta a = br_{\rm H}$, with $b \sim$10 (*Lissauer*, 1987; *Kokubo and Ida*, 1998) and

$$r_{\rm H} \equiv \left(\frac{m_1+m_2}{3m_*}\right)^{1/3}\frac{a_1+a_2}{2} \sim \left(\frac{2m}{3m_*}\right)^{1/3} a. \tag{10}$$

If an oligarch consumes all planetesimals with semimajor axes between $a - 0.5br_{\rm H}$ and $a + 0.5br_{\rm H}$, it reaches the isolation mass, $M_{\rm iso} = 2\pi a \Sigma_{\rm d} b r_{\rm H}$ (*Lissauer*, 1987):

$$\frac{M_{\rm iso}}{M_\oplus} = \frac{4\pi^{3/2}b^{3/2}}{3^{1/2}}\left(\frac{\Sigma_{\rm d}a^2}{m_*}\right) \sim 0.16\left(\frac{b}{10}\right)^{3/2}\left(\frac{a}{1{\rm AU}}\right)^{3-3\alpha/2}\left(\frac{\Sigma_{\rm d1}}{10{\rm g\ cm^{-2}}}\right)^{3/2}. \tag{11}$$

From equations (6) and (11), *Kokubo and Ida* (2002) derived the growth time of an isolated body:

$$\frac{t_{\rm grow}}{1{\rm Myr}} \simeq 0.3\left(\frac{\Sigma_{\rm d1}}{10{\rm g\ cm^{-2}}}\right)^{-9/10}\left(\frac{b}{10}\right)^{1/10}\left(\frac{a}{1{\rm AU}}\right)^{(9\alpha+16)/10}. \tag{12}$$

3.2. Observational Tests: Debris Disks

Deriving robust tests of planet formation theory requires a bridge from analytic estimates to observational predictions. Numerical simulations provide this bridge. Idealized calculations test the analytic results for the important timescales and physical processes during runaway and oligarchic growth (e.g., *Ohtsuki et al.*, 1993, 2002; *Kokubo*

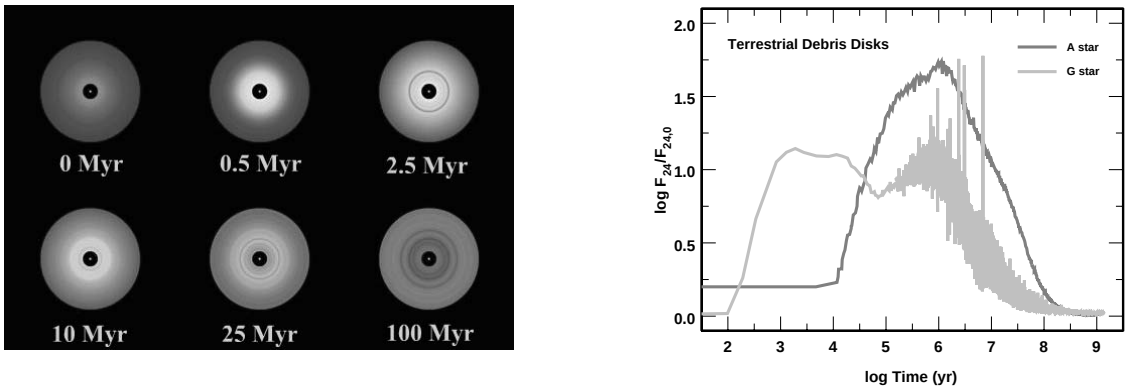

Fig. 1.— Evolution of debris disks in the terrestrial zone. For an A-type star with a luminosity of $\sim 50\ L_\odot$, the range in blackbody temperatures of planetesimals at 3–20 AU (425–165 K) is similar to the range in the Solar System at 0.4–2 AU (440–200 K). *Left panel:* Images of a disk extending from 3–20 AU around an A-type star (*Kenyon and Bromley*, 2005). The intensity scale indicates the surface brightness of dust, with black the lowest intensity and white the highest intensity. *Right panel:* Mid-IR excess for two debris disk models (*Kenyon and Bromley*, 2004b, 2005). The light grey line plots the ratio of the 24 μm flux from a debris disk at 0.4–2 AU disk relative to the mid-IR flux from a G-type star. The dark grey line shows the evolution for the A-star disk shown in the left panel.

and Ida, 1996, 1998, 2002). More complete calculations yield starting points for observational tests (*Wetherill and Stewart*, 1989, 1993; *Weidenschilling et al.*, 1997). Recent advances in computing power enable more complete simulations and promise robust tests of planet formation theories.

There are few constraints on planetesimal formation. Observations of disks in T-Tauri stars provide some evidence for grain growth (chapters by *Dutrey et al.*; *Ménard et al.*), but there is little information on the timescale for planetesimal formation (chapters by *Dominik et al.*; *Natta et al.*). Once planetesimals form, numerical simulations suggest a rapid transition from runaway growth to oligarchic growth, $\lesssim 10^5$ yr (e.g., *Wetherill and Stewart*, 1993). Near-infrared (near-IR) colors of T-Tauri stars provide some observational support for a similarly rapid transition from a dusty disk (of planetesimals) to a relatively dust-free disk (of oligarchs) (*Kenyon and Hartmann*, 1995).

Once oligarchs form, observations can provide clean tests of planet formation theory. As protoplanets stir their surroundings, collisions between planetesimals produce debris instead of mergers (*Wetherill and Stewart*, 1993; *Kenyon and Bromley*, 2002; see also *Agnor and Asphaug*, 2004; *Leinhardt and Richardson*, 2005). Debris production leads to a collisional cascade, where leftover planetesimals are ground to dust. In the terrestrial zone, dust has an equilibrium temperature of $\sim$ 200–400 K and emits radiation at wavelengths of 5–30 μm, where *Spitzer* operates.

The onset of the collisional cascade is tied to the evolution of the largest objects and the material properties of planetesimals. During oligarchic growth, $v_{\rm f} \lesssim v_{\rm esc,olig}$. Substantial debris production begins when the center of mass collision energy is comparable to the typical binding energy of a leftover planetesimal (*Wetherill and Stewart*, 1993). For equal mass leftovers, this limit yields $v_{\rm f} \approx 10\ Q_d^{1/2}$ (*Kenyon and Bromley*, 2005), where Q_d is the 'disruption' energy needed to eject roughly half of the mass of the colliding objects (*Benz and Ausphaug*, 1999):

$$Q_{\rm d} = Q_b d^{\alpha_b} + \rho_{\rm m} Q_{\rm g} d^{\alpha_{\rm g}}. \qquad (13)$$

Here, $Q_b d^{\alpha_b}$ is the bulk strength and $\rho_{\rm m} Q_{\rm g} d^{\alpha_{\rm g}}$ is approximately the gravitational binding energy. For rocky planetesimals with $\rho_{\rm m}$ = 3 g cm^{-3}, laboratory measurements and numerical simulations suggest $Q_b \approx 6 \times 10^7$ erg g^{-1}, $\alpha_b \approx -0.4$, $Q_g \approx 0.4$ erg cm^{-3}, and $\alpha_g \approx 1.25$–1.5, which yield $Q_{\rm d} \sim 10^8 - 10^9$ erg g^{-1} for 10 km objects (*Housen and Holsapple*, 1990, 1999; *Holsapple*, 1994; *Durda et al.*, 1998, 2004; *Benz and Ausphaug*, 1999; *Michel et al.*, 2001). Thus, the collisional cascade begins when $v_{\rm esc,olig} \approx 1$ km s^{-1}, corresponding to the formation of 1000 km objects.

The collisional cascade produces copious amounts of dust, which absorb and scatter radiation from the central star. Following the growth of protoplanets, the cascade begins at the inner edge of the disk and moves outward. For calculations with a solar-type central star, it takes $\sim$ 0.1 Myr for dust to form throughout the terrestrial zone (0.4–2 AU). The timescale is $\sim$ 1 Myr for the terrestrial zone of an A-type star (3–20 AU). As the collisional cascade proceeds, protoplanets impose structure on the disk (Fig. 1, left panel). Bright rings form along the orbits of growing protoplanets; dark bands indicate where a large protoplanet has swept up dust along its orbit. In some calculations, the dark bands are shadows, where optically thick dust in the inner disk prevents starlight from shining on the outer disk (*Grogan, et al.*, 2001; *Kenyon and Bromley*, 2002, 2004a, 2005; *Durda et al.*, 2004).

In the terrestrial zones of A-type and G-type stars, the dust emits mostly at mid-IR wavelengths. In calculations

with G-type central stars, formation of a few lunar mass objects at 0.4–0.5 AU leads to copious dust production in a few thousand years (Fig. 1, right panel). As protoplanets form farther out in the disk, the disk becomes optically thick and the mid-IR excess saturates. Once the orbits of oligarchs start to overlap ($\sim$ 1 Myr), the largest objects sweep the disk clear of small planetesimals. The mid-IR excess fades. During this decline, occasional large collisions generate large clouds of debris that produce remarkable spikes in the mid-IR excess (*Kenyon and Bromley*, 2002, 2005).

In A-type stars, the terrestrial zone lies at greater distances than in G-type stars. Thus, debris formation in calculations with A-type stars begins later and lasts longer than in models with G-type stars (Fig. 1, right panel). Because the disks in A-type stars contain more mass, they produce larger mid-IR excesses. At later times, individual collisions play a smaller role, which leads to a smoother evolution in the mid-IR excess with time (see *Kenyon and Bromley*, 2005). Although the statistics for G-type stars is incomplete, current observations suggest that mid-IR excesses are larger and last longer for A-type stars than for G-type stars (see *Rieke et al.*, 2005 and the chapter by *Meyer et al.*).

Collisional cascades and debris disk formation may impact the final masses of terrestrial planets. Throughout oligarchic growth, $\sim$ 25% to 50% of the initial mass in planetesimals is converted into debris. For solar-type stars, the disk is optically thick, so oligarchs probably accrete the debris before some combination of gas drag, Poynting-Robertson drag, and radiation pressure remove it. In the disks of A-type stars, the debris is more optically thin. Thus, these systems may form lower mass planets per unit surface density than disks surrounding less massive stars. Both of these assertions require tests with detailed numerical calculations.

3.3. Observational Tests: Cosmochemistry

Radioactive dating provides local tests of the timescales for oligarchic and chaotic growth (chapter by *Wadwha et al.*). The condensation of Ca-Al-rich inclusions and formation of chondrules at a solar age $t_\odot \sim$ a few Myr indicate short timescales for planetesimal formation (and perhaps runaway growth). At later times, lunar samples suggest the Moon was fully formed at $t_\odot \sim$ 50 Myr (e.g., *Halliday et al.*, 2000; *Wood and Halliday* 2005). The difference between the abundance of radioactive Hf in primitive meteorites and in the Earth's mantle suggests that the Earth's core differentiated $\sim$ 30 Myr after the first CAI condensed out of the solar nebula (*Yin et al.* 2002). The Hf data suggest the Martian core probably formed in $\sim$ 15 Myr (*Jacobsen* 2005). With U-Pb data implying a somewhat later time, $\sim$ 65-85 Myr (*Halliday* 2004), the Hf-W timescale probably measures the time needed to form most of the core, while the U-Pb timescale refers to the last stages of core segregation (*Sasaki and Abe*, 2005; *Wood and Halliday* 2005).

For planet formation theory, including the giant impact model for the formation of the Moon, these data suggest (i) the first oligarchs formed at $t_\odot \lesssim$ 10 Myr, (ii) the era of chaotic growth occured at $t_\odot \sim$ 15–80 Myr, and (iii) massive oligarchs sufficient to produce the Moon from a giant impact existed at $t_\odot \sim$ 40–50 Myr. To confront the models with these results, we now consider the most recent numerical models of chaotic growth.

4. NEW SIMULATIONS OF CHAOTIC GROWTH

Chaotic growth is the most delicate phase of terrestrial planet formation. In the current picture, oligarchs in roughly circular orbits evolve into a chaotic system and begin colliding. Once these giant collisions produce several Earth-mass planets, the oligarchs evolve back into an orderly system with roughly circular orbits. Recent research efforts focus on (i) N-body simulations of oligarchs, to derive the frequency of Earth-like planets (including the abundance of water) as a function of initial conditions (Section 4.1), (ii) hybrid simulations of planet growth, to understand how the evolution depends on the mass in leftover planetesimals and fragmentation processes (Section 4.2), and (iii) N-body simulations where secular resonances dominate the evolution of oligarchs, to investigate how the masses and orbital properties of planets depend on the relative mass in the disk and in gas giant planets (Section 4.3).

4.1. N-Body Calculations

N-body simulations of chaotic growth begin with an ensemble of N oligarchs distributed throughout the terrestrial zone. The oligarchs have an initial range of masses m_i, an initial surface density distribution (eq. 3), initial spacing b, initial spin distribution, and, in some cases, gas giants with initial masses and orbits or a gas disk with an initial surface density (eq. 4). To understand the range of possible outcomes, an ensemble of calculations with the same set of initial conditions yields statistical estimates for the physical properties of planets and leftover oligarchs.

Most simulations adopt a standard model with $\Sigma_{\rm d1} \sim$ 8–12 g cm^{-2}, $\alpha = 3/2$, $b \simeq 10$, and $\rho_{\rm m} = 3$ g cm^{-3} (e.g., *Chambers and Wetherill*, 1998; *Agnor et al.*, 1999; *Chambers*, 2001; *Kokubo et al.* 2006a). Here, we summarize aspects of *Kokubo et al.* (2006a), who consider a baseline model with $\Sigma_{\rm d1}$ = 10 g cm^{-2}, and note similarities and differences between this calculation and other published results. The left panel of Fig. 2 shows one run of out 200 with a variety of $\Sigma_{\rm d}$ from *Kokubo et al.* (2006a).

In this standard case, N-body simulations yield two (2 ± 0.6) major planets with 80% of the initial mass. The masses of the largest and second largest planets are $1.27 \pm 0.25\ M_\oplus$ and $0.66 \pm 0.23\ M_\oplus$. The planets have orbital elements (a, e, i) = (0.75$\pm$0.20 AU, 0.11 ± 0.07, 0.06 ± 0.04, largest) and (1.12 ± 0.53, 0.12 ± 0.05, 0.10 ± 0.08, second largest). For comparison, Table 1 (left column) lists the orbital data for the Solar System, with a and e averaged over 10 Myr from J2000 and i measured in radians relative to the invariable plane. Aside from e and i, these calculations account for the general appearance of the inner Solar System.

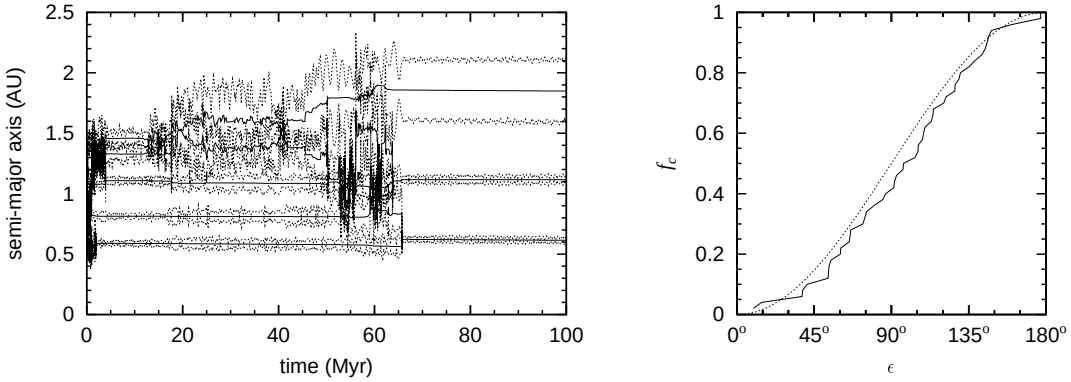

Fig. 2.— N-body results for chaotic growth. *Left panel:* A single simulation from (*Kokubo et al.*, 2006a; their Fig. 1). The simulation starts with 16 protoplanets. The curves show the semimajor axes (solid lines) and peri- and aphelion distances (dashed lines) as a function of time. *Right panel:* Cumulative histogram of the obliquity for an ensemble of calculations as in the left panel (from *Kokubo et al.* 2006b, in preparation). The solid line shows results (ϵ in deg) for the largest planet from 50 calculations. The dotted line shows a random distribution, where $2f_c = \int_0^\epsilon \sin\epsilon d\epsilon$.

The obliquity distribution derived from the N-body calculations provides another probe of terrestrial planet formation. In general, the results are similar to the distribution expected for planets formed from an ensemble of giant impacts with random spins (*Agnor et al.*, 1999; *Chambers*, 2001). The right panel of Fig. 2 shows a cumlative fraction of the obliquities of the largest planets from *Kokubo et al.* (2006b, in preparation). The derived distribution is roughly random. Any comparison with the Solar System requires much care. The obliquities of terrestrial planets today ($\sim$ perpendicular to the orbital planes) have evolved considerably due to spin-orbit coupling, tidal interactions, and perhaps other physical processes (e.g., *Ward*, 1973; *Lissauer and Kary*, 1991).

4.1.1. Dependence on conditions for the disk

Because every set of initial conditions requires many simulations to derive a statistical measure of possible outcomes, measuring the sensitivity of outcomes to the initial conditions is a major task. Recent advances in computing speed make this problem tractable. *Kokubo et al.* (2006a) derive statistical uncertainties from 200 simulations. Within a few years, larger sets of calculations will improve these estimates. For calculations without an external perturber (a giant planet or binary companion star), there is fairly good agreement in how outcomes depend on the total mass in oligarchs $M_{\rm tot}$, the shape of the surface density distribution, the initial spacing of oligarchs, and the bulk properties (mass density, water content, rotational spin, etc) of the oligarchs. Better sampling of available phase space will provide better constraints on the outcomes.

The growth of terrestrial planets is most sensitive to the initial mass in solid material and the radial distribution of this material in the disk. For simulations with $\Sigma_{\rm d1}$ = 1–100 g cm^{-2}, α = 0–2.5, b = 6–12, and $\rho_{\rm m}$ = 3–6 g cm^{-3}, larger planets form in more massive disks. Low mass disks produce a larger number of low mass planets (e.g., *Wetherill*, 1996; *Chambers and Cassen*, 2002; *Raymond et al.*, 2005a; *Kenyon and Bromley*, 2006; *Kokubo et al.*, 2006a). *Kokubo et al.* (2006a) derive (see Fig. 3)

$$\langle n \rangle \sim 3.5 \left(\frac{M_{\rm tot}}{2M_\oplus} \right)^{-0.15}. \quad (14)$$

for the average number of planets and

$$\langle M_1 \rangle \sim 1.0 \left(\frac{M_{\rm tot}}{2M_\oplus} \right)^{1.1} M_\oplus \sim 0.5 M_{\rm tot}, \quad (15)$$

$$\langle M_2 \rangle \sim 0.60 \left(\frac{M_{\rm tot}}{2M_\oplus} \right)^{0.98} M_\oplus \sim 0.3 M_{\rm tot}. \quad (16)$$

for the masses of the largest (M_1) and the second largest (M_2) planets. The dependence of $\langle n \rangle$ and $\langle M_{1,2} \rangle$ on the surface density is weaker than for oligarchic growth (-1/2 and 3/2, respectively). This may be because the growth mode is more global, being no longer just scaled by the local feeding zone. The location of the largest planet (a_1) is independent of $\Sigma_{\rm d1}$ in their simulation range. They obtained a numerical fit of $\langle a_1 \rangle \sim 0.90 (\bar{a}/1{\rm AU})^{1.7}$ AU, where, $\bar{a}$ is the mean semimajor axis of protoplanets. The second planet is further separated in response to the stronger repulsion as $\Sigma_{\rm d1}$ increases. For the same reason, the eccentricities and inclinations of the largest planets increase with $\Sigma_{\rm d1}$. Qualitatively, these results can be understood as follows: In more massive disks, oligarchs have larger isolation masses (eq. 11) and thus merge to produce more massive planets. More massive planets have larger Hill radii and thus clear out larger volumes, yielding fewer planets in stable orbits. Conversely, lower-mass disks produce lower-mass oligarchs (see also *Kenyon and Bromley*, 2006).

The radial surface density gradient, α, sets the final radial mass distribution of planets and their composition. Calculations with small α produce larger, more well-mixed planets at larger semimajor axes than calculations with

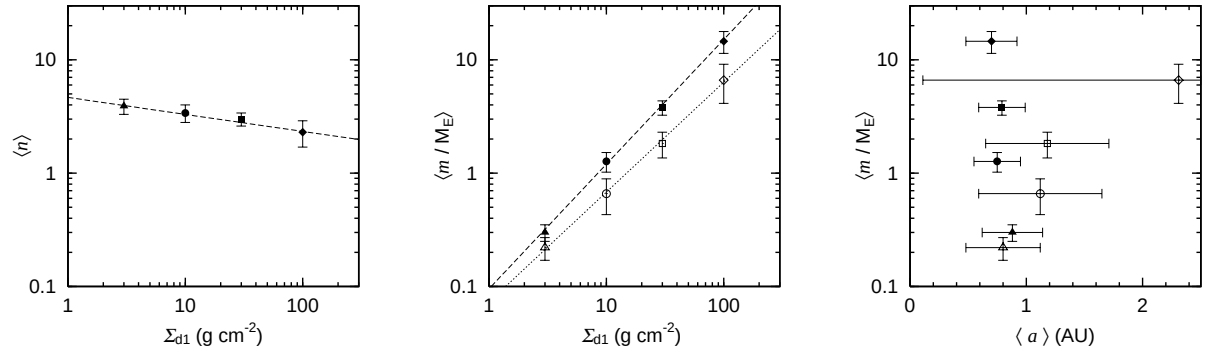

Fig. 3.— Results of chaotic growth for $\Sigma_{\rm d1} = 3$ (triangles), 10 (circles), 30 (squares), and 100 (diamonds) $\rm g\ cm^{-2}$. *Left panel:* Average number of planets as a function of surface density (*Kokubo et al.*, 2006a; their Fig. 5). *Center panel:* Masses of the largest (filled circles) and second largest (open circles) planets as functions of surface density (*Kokubo et al.*, 2006a; their Fig. 7). *Right panel:* Masses of the largest (filled circles) and second largest (open circles) planets as a function of semimajor axis (*Kokubo et al.*, 2006a; their Fig. 6). The error bars show standard deviations derived from 20 calculations for 100–300 Myr. The lines correspond to the least-squares fits.

larger α (*Chambers and Cassen*, 2002; *Raymond et al.*, 2005a; *Kokubo et al.*, 2006a). For fixed $M_{\rm tot}$, the number and masses of terrestrial planets are fairly insensitive to α. When the surface density gradient is shallow (small α), there is relatively more mass at larger heliocentric distances, which leads to the production of more massive oligarchs. These oligarchs are less isolated, are easily scattered throughout the computational grid, and thus radially well-mixed. In calculations with steep surface density gradients (large α), most of the mass is concentrated in a small range of heliocentric distances, so oligarchs are more isolated and harder to scatter throughout the grid. Thus, shallow surface density gradients allow for easier water delivery to the innermost terrestrial planets from oligarchs at large semimajor axes (e.g., *Raymond et al.*, 2005a).

The orbital e and i are sensitive to the total mass in oligarchs (e.g., *Kokubo et al.*, 2006a) and to the initial mass range in oligarchs (e.g., *Chambers*, 2001). For a fixed mass range and number of oligarchs, larger $M_{\rm tot}$ can produce larger e and i. A mass range allows dynamical friction to reduce e and i of the most massive bodies; at the same time, such simulations tend to produce more planets in the end. Because N-body calculations are still restricted in the maximum number of bodies that can be evolved for long times, detailed simulations of the transition between oligarchic and chaotic growth (i.e. starting with a significant fraction of the mass still in planetesimals) remain challenging to perform, and it is unclear what role leftover planetesimals play in the final e and i distributions of planets. We revisit this issue in Section 4.2.

Despite the uncertainty in the final e and i, most Earth-mass planets form close to 1 AU (*Chambers*, 2001; *Raymond et al.*, 2005a; *Kokubo et al.*, 2006a). Massive planets are less likely to form at $a \lesssim 0.5$ AU because typical surface density profiles do not have enough mass to produce a planet as large as the Earth. At larger radii, perturbations from Jupiter tend to inhibit formation, as discussed next.

4.1.2. Pertubations from gas giant planets

Long-range gravitational interactions with gas giant planets beyond 3–5 AU impact the formation of terrestrial planets in two ways. If gas giants are fully-formed before the runaway growth phase, stirring by gas giants can slow runaway growth and delay oligarchic growth. Once oligarchs form, stirring promotes orbit crossing and the growth of oligarchs from giant impacts. The final configuration and composition of terrestrial planets then depends on the masses and orbital parameters of gas giants.

For gas giants in circular orbits, the importance of long-range stirring depends on the Hill radii of the planets. Because Jupiter has $r_{\rm H} \sim 0.1\ a$ and large dynamical interactions require separations less than 5–6 $r_{\rm H}$, a Jupiter at 5–6 AU (as in the Solar System) has little impact on planet formation at 1 AU. However, Jupiter is effective at removing material outside 2 AU and effectively ends planet formation in the asteroid belt once it reaches its final mass (*Wetherill*, 1996; *Chambers and Wetherill*, 1998; *Levison and Agnor*, 2003). A Jupiter at 3.5 AU limits the formation of terrestrial planets outside of 1 AU; a Jupiter at 10 AU allows formation of terrestrial planets in the asteroid belt. Because $r_{\rm H}$ scales with mass, more massive gas giants prevent planet formation throughout the terrestrial zone.

For elliptical orbits, the dynamical reach of the gas giant for gravitational scattering is $\sim$ 5–6 $r_{\rm H} + ae$. Elliptical orbits also lead to perturbations from mean-motion resonances and secular interactions. Thus gas giants on elliptical orbits affect planet formation over larger volumes (*Chambers and Cassen*, 2002; *Levison and Agnor*, 2003; *Raymond et al.*, 2004). For calculations with $e_{\rm J,S}$ = 0.1, Jupiter and Saturn rapidly clear the asteroid belt and prevent "wetter" oligarchs from colliding with drier oligarchs inside 1.5 AU. Thus, a massive, wet, and stable Earth depends on the fairly circular orbits of Jupiter and Saturn.

4.1.3. Extrasolar systems

The discovery of extrasolar planets with masses ranging from Neptune up to 10–20 Jupiter masses opens up amazing vistas in calculations of terrestrial and gas giant planet formation. For terrestrial planets, the main issue is whether an extrasolar planetary system has enough phase space to allow the formation of a stable planet. There are two broad cases, (i) wide systems where the gas giants (or companion stars) have semimajor axes $a \gtrsim$ 1–2 AU and (ii) compact systems where close-in gas giants have $a \lesssim 0.1$ AU.

Terrestrial planets can form in wide systems that parallel the structure of the Solar System (*Heppenheimer*, 1978; *Marzari and Scholl*, 2000; *Kortenkamp and Wetherill*, 2000; *Kortenkamp et al.*, 2001; *Thébault et al.*, 2002). In ϵ Eri and 47 UMa, terrestrial planets can form at $\lesssim 0.8$ AU, well inside the orbits of the gas giant planets, but these planets may not be stable (*Jones et al.*, 2001; *Thébault et al.*, 2002; *Laughlin et al.*, 2002). Stable terrestrial planets can form around both components of the wide binary α Cen (*Quintana et al.*, 2002; *Barbieri et al.*, 2002). Unlike the Solar System, uncertainties in the orbital parameters of extrasolar gas giants complicates identifying stable regions for lower mass planets. As new observations reduce these uncertainties, we will have a better picture of possible outcomes for terrestrial planet formation in specific systems.

For systems with close-in gas giants, terrestrial planet formation depends on the availability of material and the orbital parameters of the gas giants. Current models suggest that close-in gas giants form at 5–10 AU and then migrate inward (chapter by *Papaloizou et al.*). Gas giant migration through the terrestrial zone removes protoplanets, scattering them into the outer solar system or pushing them into orbits closer to the central star. The amount of material left behind depends on the physics of the migration episode (e.g., *Armitage*, 2003; *Fogg and Nelson*, 2005). However, most calculations suggest that planets can form during or after migration. The masses and orbits of these planets then depend on the mass and orbit of the close-in giant planet (e.g., *Raymond et al.*, 2005b; *Zhou et al.*, 2005).

4.1.4. Water Delivery

For conditions in most protosolar nebula models, the disk temperature at 1 AU is too large for volatile molecules to condense out of the gas. Thus, current theory requires a system to deliver water to the Earth. The relatively high D/H ratio of the Earth's oceans, ~ 7 times the ratio expected in the protosolar nebula, also suggests a delivery system rather than direct absorption (see, however, *Abe et al.*, 2000; *Drake*, 2005). There are two possible sources of water outside the Earth's orbit, the asteroid belt, where Jupiter effectivel crushes and scatters large objects into the inner solar system (e.g., *Morbidelli et al.*, 2000) and the Kuiper belt, where interactions with Neptune and then Jupiter may allow icy objects from the outer Solar System to collide with the Earth (e.g., *Levison et al.*, 2001; Gomes et al., 2005). Current evidence may favor the asteroid belt, where the D/H ratio derived from carbonaceous chondrites is closer to the ratio in Earth's oceans than the ratio derived from comets (see *Balsiger et al.*, 1995; *Meier et al.*, 1998; *Bockelee-Morvan et al.*, 1998; *Dauphas et al.*, 2000; *Drake and Righter*, 2002).

Raymond et al. (2004, 2005b) calculate how plantesimals or oligarchs from the asteroid belt deliver water to planets near 1 AU (see also *Lunine et al.*, 2003). Due to the stochastic nature of collisions with massive objects, these results suggest that the water content of terrestrial planets is highly variable. The water abundance on Earth, Venus, and Mars is also sensitive to Jupiter's efficiency at cleaning material out of the asteroid belt.

4.1.5. Eccentricity damping

In addition to water delivery, the final e and i of terrestrial planets are important targets for N-body models. Aside from leftover small oligarchs, two processes can circularize the orbits of terrestrial planets. If a large fraction of the mass in leftover planetesimals cycles through the collisional cascade (Section 3.2), small dust grains might also damp the eccentricities of planets (*Goldreich et al.*, 2004). Because the mass of a single grain is much less than the mass of a single planetesimal, a small total mass in grains can effectively damp massive oligarchs. *Goldreich et al.* (2004) note that oligarchs might also accrete grains more rapidly than leftover planetesimals, shortening the chaotic growth phase and promoting circular orbits. Kenyon and Bromley (2006, in preparation) are testing this possibility.

Interactions with the residual gas disk also damp the eccentricities of terrestrial planets (*Artymowicz*, 1993; *Agnor and Ward 2002*; *Kominami and Ida*, 2002; *Tanaka et al.* 2002; *Tanaka and Ward*, 2004). Although gas drag on growing oligarchs is small, coupling between a planet and the Lindbald and corotation resonances of the gas disk (e.g., *Goldreich and Tremaine*, 1980) can be significant. For $\alpha = 3/2$, the tidal torques damp e on a timescale

$$\tau_{\rm damp} \simeq \left(\frac{m}{M_\odot}\right)^{-1} \left(\frac{\Sigma_{\rm g} a^2}{M_\odot}\right)^{-1} \left(\frac{c_s}{a\Omega_{\rm K}}\right)^4 \Omega_{\rm K}^{-1}, \quad (17)$$

$$\simeq 5 \times 10^2 \left(\frac{m}{M_\oplus}\right)^{-1} \left(\frac{\Sigma_{\rm g1}}{\Sigma_{\rm MMSN}}\right)^{-1} \left(\frac{a}{1{\rm AU}}\right)^2 {\rm yr}$$

where $c_{\rm s}$ is the sound velocity. Because interactions with the disk also drag the planet towards the Sun, damping the eccentricity without losing the planet requires a "remnant" gas disk with a small fraction of the mass in a MMSN.

In a large set of numerical simulations, *Kominami and Ida* (2002, 2004) included this gravitational drag using

$$\mathbf{f}_{i,{\rm grav}} = -\frac{(\mathbf{v} - \mathbf{v}'_{\rm K})}{\tau_{\rm damp}} \exp(-t/\tau_{\rm deple}), \quad (18)$$

where $\mathbf{v}'_{\rm K}$ is the Keplerian velocity and $\tau_{\rm deple}$ is the gas disk depletion timescale. This form is motivated by observations of young stars, where the gas disk disappears on a timescale of 1–10 Myr. Although damping with the residual gas disk is effective, these simulations tend to produce

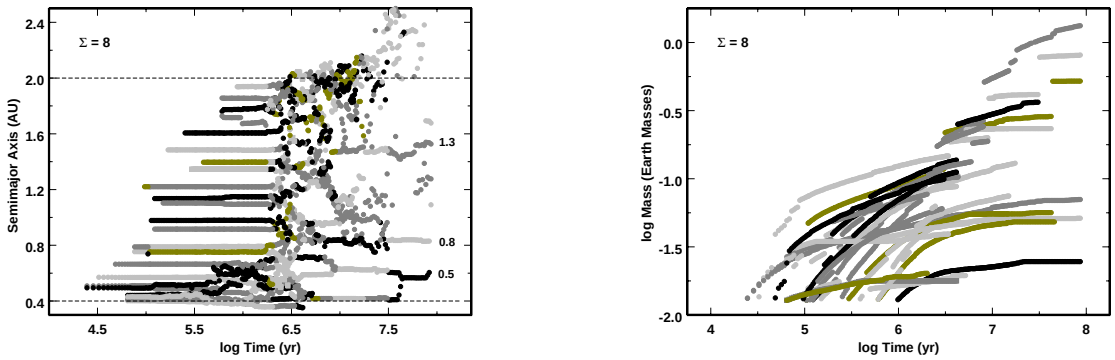

Fig. 4.— Evolution of oligarchs in the terrestrial zone. The hybrid calculation starts with 1 km planetesimals ($\rho_{\rm m}$ = 3 g cm^{-3}) in a disk with $\Sigma_{\rm d1}$ = 8 g cm^{-2} and α = 1. The planetesimal disk contains 40 annuli extending from 0.4 AU to 2 AU. *Left panel:* The time evolution of semimajor axis shows three phases that start at the inner edge of the grid and propagate outward: (i) after runaway growth, isolated oligarchs with $m \gtrsim 4 \times 10^{25}$ g enter the grid; (ii) oligarchs develop eccentric orbits, collide, and merge; and (iii) a few massive oligarchs eventually contain most of the mass and develop roughly circular orbits. The legend indicates masses (in $M_\oplus$) for the largest oligarchs. *Right panel:* The mass evolution of oligarchs shows an early phase of runaway growth (steep tracks) and a longer phase of oligarchic growth (relatively flat tracks), which cluminates in a chaotic phase where oligarchs grow by captures of other oligarchs (steps in tracks).

many low mass planets. As the gas disk disappears, these planets go through another chaotic growth phase that produces large e as in the N-body simulations of Section 4.1.

4.2. Hybrid Calculations

Standard N-body calculations of chaotic growth have several successes and failures. The simulations produce 2 planets with (m, a) similar to Earth and Venus and several more with (m, a) similar to Mars and Mercury. While the models can explain the inverse relation between m and e and provide some understanding of the solid-body rotation rates, they fail to account for the nearly circular, low inclination orbits of the Earth and Venus. In calculations with many low mass oligarchs, *Chambers* (2001) noted that dynamical friction helped to circularize orbits of Earth-mass planets. This result suggests that calculations including leftover planetesimals, which contain roughly half the mass at the onset of chaotic growth, might yield more circular orbits for Earth-mass planets. To test this and other ideas, *Bromley and Kenyon* (2006) developed a hybrid, multiannulus coagulation + N-body code that follows the joint evolution of planetesimals and oligarchs.

In the hybrid code, a coagulation algorithm treats the evolution of planetesimals into oligarchs using particle-in-a-box techniques (*Kenyon and Bromley*, 2004a). A direct N-body calculation follows the evolution of oligarchs into planets. The 'promotion mass' $m_{\rm pro}$ sets the transition from the coagulation grid to the N-body grid; for most applications $m_{\rm pro} \approx 10^{25}{\rm g}\ (\Sigma_{\rm d1}/8\ {\rm g\ cm^{-2}})$ (*Kenyon and Bromley*, 2006). This code uses the particle-in-a-box and Fokker-Planck formalisms to treat the interactions between oligarchs in the N-body grid and planetesimals in the coagulation grid. *Bromley and Kenyon* (2006) describe tests of the hybrid code and show that it reproduces several previous calculations of terrestrial planet formation (*Weidenschilling et al.*, 1997; *Chambers*, 2001). *Kenyon and Bromley* (2006) describe how the results depend on $m_{\rm pro}$.

Fig. 4 shows the evolution of oligarchs in one evolutionary sequence using the hybrid code. Following a short runaway growth phase, large objects with $m \gtrsim m_{\rm pro}$ appear in a wave that propagates out through the planetesimal grid. As these oligarchs continue to accrete planetesimals, dynamical friction maintains their circular orbits and they evolve into 'isolated' objects. Eventually, large oligarchs start to interact dynamically at the inner edge of the grid; this wave of chaotic interactions moves out through the disk until all oligarchs interact dynamically. Once a few large oligarchs contain most of the mass in the system, dynamical friction starts to circularize their orbits. This process excites the lower mass oligarchs and leftover planetesimals, which are slowly accreted by the largest oligarchs.

Comparisons between the results of hybrid and N-body calculations show the importance of including planetesimals in the evolution. Both approaches produce a few terrestrial mass planets in roughly circular orbits. Because dynamical friction between leftover planetesimals and the largest oligarchs is significant, hybrid calculations produce planets with more circular orbits than traditional N-body calculations. In most hybrid calculations, lower mass planets have more eccentric orbits than the most massive planets, as observed in the Solar System. In both approaches, the final masses of the planets grow with the initial surface density; the number of planets is inversely proportional to surface density. However, the overall evolution is faster in hybrid calculations: oligarchs start to interact earlier and produce massive planets faster.

In hybrid calculations, the isolation mass and the number of oligarchs are more important as local quantities than as global quantities. As waves of runaway, oligarchic, and chaotic growth propagate from the inner disk to the outer disk, protoplanets growing in the inner disk become isolated at different times compared to protoplanets growing in the outer disk. Thus, the isolation mass in hybrid models is a function of heliocentric distance, initial surface density, and *time*, which differs from the classical definition (eq. 11). It is not yet clear how this change in the evolution affects the final masses and orbital properties of terrestrial planets.

4.3. The Role of Gas Depletion in the Final Assembly of Terrestrial Planets

The Solar System is full of resonances that produce delicate structure in planetary orbits. In the asteroid belt, for example, there are few objects in the n:m orbital resonances, where an asteroid makes n revolutions of the Sun for every m revolutions of Jupiter. Because asteroids orbit within 5–6 $r_{\rm H,J} \sim$ 2.5–3 AU of Jupiter's orbit, Jupiter constantly stirs up the asteroids and modifies their orbits. For asteroids in orbital resonance, Jupiter stirring always peaks at the same orbital phase, which leads to a secular (instead of random) change in orbital parameters and eventually ejection from the resonance. In contrast, the Trojan satellites of Jupiter occupy the 1:1 resonance, roughly the stable L_4 and L_5 points in the restricted three body problem. Many KBOs occupy the n:m orbital resonances with Neptune, where they are also relatively safe from Neptune's gravitational perturbations (*Chiang et al.*, this volume).

Resonances are also an important part of planet formation. When large planets start to form, the massive gaseous disk limits their gravitational reach. As the disk dissipates, planets begin to shape their surroundings. For terrestrial planets, the ν_5 resonance – effectively the semimajor axis where the precession of the line of apsides of an orbit is in phase with the precession of Jupiter's orbit – can play an important role in the transition from oligarchic growth to chaotic growth. As the disk dissipates, the ν_5 resonance sweeps from Jupiter's orbit through the terrestrial zone to its current location at $\sim$ 0.6 AU (*Ward et al.*, 1976), transforming a system of isolated oligarchs into a chaotic system of merging oligarchs with overlapping orbits (*Nagasawa et al.*, 2000). As chaotic growth ends, the last remnants of the disk circularize the orbits of the remaining planets. To illustrate how this process might produce the architecture of the inner Solar System, we now describe this dynamical shake-up model (*Nagasawa et al.*, 2005; *Lin et al.*, 2006, in preparation; *Thommes et al.*, 2006, in preparation).

Several features of the sweeping ν_5 resonance make it an attractive feature of terrestrial planet formation. The resonance passes through the terrestrial region almost independently of the details of disk depletion (*Nagasawa et al.*, 2000). It is also largely independent of the disk radial surface density profile. For cases when Jupiter and Saturn have their current orbits, Fig. 5 shows that the position of

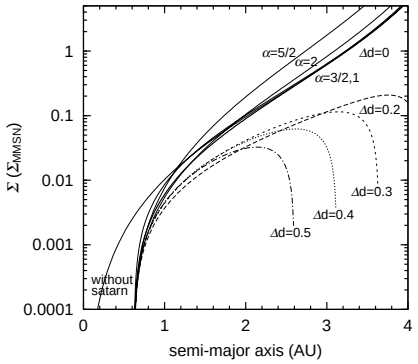

Fig. 5.— Evolution with disk depletion of the ν_5 resonances for different power laws (α =1, 3/2, 2, and 5/2) of the surface density of the gas disk (solid lines). The edges of the gaps are located at $a_{\rm J}(1 \pm \Delta d)$ and $a_{\rm S}(1 \pm \Delta d)$. We examine Δd= 0, 0.2, 0.3, 0.4, and 0.5 in the case of $\alpha = 3/2$.

the resonance is not sensitive to α or to the presence of gaps in the disk. When the Jovian planets produce gaps in the disk, the resonance occurs once the planetary perturbation surpasses the disk's perturbation and the rotation of periastra of the protoplanets changes to prograde from retrograde (*Ward* 1981). Although the timing of resonance passage is slightly delayed, gap formation does not significantly modify the overall evolution of the resonance inside 2 AU.

In addition to exciting e, the sweeping secular resonance can trap protoplanets and push them inward. As the resonance sweeps across a planet, it reduces the angular momentum without changing energy. The resonance rapidly excites e without changing a. As gravitational drag damps e, it extracts energy from the orbit and the orbits shrinks. Under the right conditions, the planet keeps pace with the sweeping resonance (*Nagasawa et al.* 2005; see below).

4.3.1. Basic Calculation

To perform numerical simulations with sweeping secular resonances, *Thommes et al.* (2006, in preparation) begin with an algorithm based on the SyMBA symplectic integrator (*Duncan et al.* 1998). They add a dissipational force to include resonant planet-disk interactions and modify the central force to include the gravitational potential of the disk on the precession rates of the embedded protoplanets. The dissipation is an extra radial acceleration (eq. 18), which changes the energy, but not the angular momentum, of an orbit. Simulations including the much smaller azimuthal component of eq. 18 differ negligibly.

These calculations begin with an analog of the inner Solar System at a stage when all objects are isolated from their neighbors. The terrestrial region, 0.5–3 AU, is seeded with an ensemble of oligarchs in nearly circular orbits with $\Sigma_{\rm d1} = 7 {\rm g\,cm^{-2}}$ and $\alpha = 1$ in eq. 3. The oligarchs have separations of 10 $r_{\rm H}$ (*Kokubo and Ida* 2000), which yields objects ranging in mass from several times $10^{-2}\,M_\oplus$ at 0.5 AU to several times $10^{-1}\,M_\oplus$ at 3 AU. A "proto-

Jupiter" and "proto-Saturn" start with 30 $M_\oplus$ and e = 0.075 at their current semimajor axes (5.2 and 9.5 AU), which roughly corresponds to their states just prior to accretion of a gaseous envelope. The model assumes gas accretion at a linear rate sufficient for Jupiter (Saturn) to reach its current mass at 1.5×10^5 yr (5×10^5 yr; see *Pollack et al.* 1996). Although this prescription assumes a strong coincidence between the formation times of Jupiter and Saturn, Fig. 5 shows that Saturn has little effect on the evolution.

For the gas, the calculations assume an exponentially decaying power-law surface density:

$$\Sigma_{\rm g} = 2000 \left(\frac{r}{1\,{\rm AU}}\right)^{-1} \exp\left(\frac{-t}{5{\rm Myr}}\right) {\rm g\,cm^{-2}} \qquad (19)$$

with a flared disk scale height (*Hayashi* 1981)

$$h = \frac{\sqrt{2} c_s}{\Omega_{\rm K}} \sim H_1 \left(\frac{r}{1\,{\rm AU}}\right)^{5/4}, \qquad (20)$$

where H_1 is the scale height at 1AU. The models adopt $H_1 = 0.05$ AU as the standard case and also examine $H_1 =$ 0.04 and 0.06 AU. Although the location of the secular resonance is independent of the mechanism for gas dissipation, the depletion timescale is important. When the gas disk inside Jupiter's orbit dissipates rapidly, the gas cannot damp e and i as the resonance moves inward. Unless there is another source of damping, such as dynamical friction due to leftover planetesimals or the collisional cascade, the final e and i of the terrestrial planets remain large.

Fig. 6 shows a standard simulation. The resonance shakes up the orbits of the protoplanets and pushes them inward, leading to orbit-crossing and many mergers. As the resonance sweeps inward, it leaves behind a Mars-mass object (t $\sim$ 20 Myr) with a semimajor axis close to that of Mars. A little later, an Earth-mass object leaves the resonance at $a \sim 1$ AU; a second object of similar mass follows the resonance almost to 0.6 AU. Both massive objects have small e, comparable to Earth and Venus. Thus, the model yields a good approximation of the present-day inner Solar System in $\sim$ 25 Myr, when "Earth" and "Venus" suffer their last impact with another protoplanet.

The timing of the formation of the Mars, Earth, and Venus analogs in this model is consistent with recent cosmochemical evidence suggesting that the Mars core is complete before the Earth's core (Section 3.3). Although this simulation has no analog to a Moon-forming giant impact at 40–50 Myr, other simulations have at least one collision after the secular resonance passes through the system. Thus, the timing of the Moon's formation is not a strong constraint on the dissipation timescale. Simulations also indicate that the disk depletion time must exceed $\tau_{\rm depl} \approx 3$ Myr; otherwise, there is not enough gas left to damp eccentricities once planets reach $m \sim M_\oplus$.

In these models, ν_5 drives material from the asteroid belt into the inner solar system. Thus, the dynamical shake-up model is more effective at delivering water to the Earth than

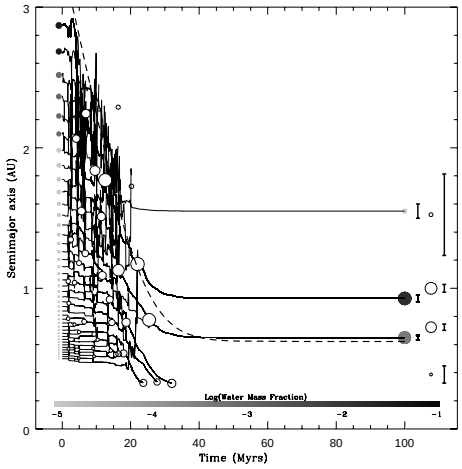

Fig. 6.— A simulation of secular resonance sweeping with collisional evolution. Initial protoplanet semimajor axes and masses are shown at left (solid circles, area $\propto$ mass). Each body's semimajor axis is then plotted as a function of time, together with any mergers that occur (open circles, area $\propto$ merger product). The path of the ν_5 resonance is also shown (dashed line). Final semimajor axes and masses (solid circles, area $\propto$ mass) are shown on the right side, with the vertical bars indicating the final peri- and apocenter locations of each. For comparison, the present-day Solar System planets are shown at far right (open circles) together with their eccentricities. Also, three different initial water abundances are adopted for the protoplanets: 10^{-5} inside 2 AU, 5×10^{-2} outside 2.5 AU, and 10^{-3} in between. The shading of the final planets indicates their resultant water content.

gravitational scattering alone. Fig. 6 shows that most of the material incorporated into the Earth analog originated beyond 2 AU, where water is more abundant. The Mars analog also forms out of wet material, while the Venus analog contains drier material within 1.5 AU.

4.3.2. Variations in Outcomes

Fig. 7 shows results for multiple 100 Myr calculations with a variety of initial conditions. The size of the circle is proportional to $m^{1/3}$. Roughly 75% to 80% of the calculations yield planets with $e \lesssim 0.1$. A slightly smaller fraction, $\sim$ 70%, form 3–4 planets. In other simulations, a smaller merger efficiency during the gaseous stage leaves behind more than 3–4 planets. Some systems become unstable after disk depletion and produce planets with $0.1 \lesssim e \lesssim 0.2$. Many configurations with more than 5 planets at 100 Myr will probably develop large e within 1–5 Gyr.

Secular resonant trapping tends to migrate protoplanets inward with the ν_5 resonance (Fig. 6). To maintain resonant trapping *Nagasawa et al.* (2005) derived

$$\left(\frac{a}{1{\rm AU}}\right)^4 \gtrsim 26 \left(\frac{e_{\rm J}}{0.05}\right)^{-2} \left(\frac{m}{M_\oplus}\right)^{-1} \left(\frac{t_{\rm depl}}{1{\rm Myr}}\right)^{-1}. \qquad (21)$$

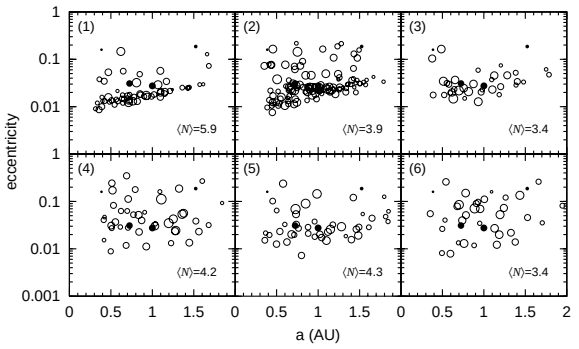

Fig. 7.— The final eccentricity vs semimajor axis of planets with different parameters. The resultant Jovian eccentricity is ∼0.07 (top panels) and ∼0.035 (bottom panels). The damping timescale is $\hat{\tau}_e = 2$ (left panels), 5 (middle panels), 10 (right panels), where $1000\hat{\tau}_e = \tau_{\rm damp}(m/M_\oplus)(a/1{\rm AU})^{-3/2}$ yr. Panel 2 consists of 30 runs. Other panels consist of 10 runs. The average number of formed planets in one run is also shown in the figures. Filled circles are current terrestrial planets.

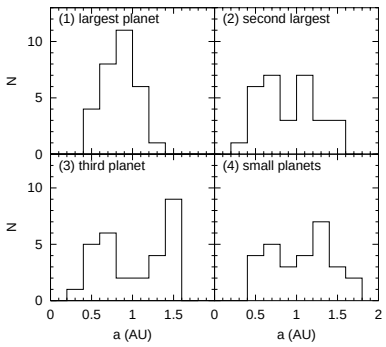

Fig. 8.— The semimajor axis histogram of (1) the largest planet in a simulation, (2) the second largest planet, (3) the third planet and (4) smaller planets. The averaged masses of them are 1.26, 0.85, 0.39, 0.23 $M_\oplus$, respectively. The largest planet has a peak at about 1 AU.

The condition for the isolated protoplanet is $a > 2$ AU with the parameters we used in simulations and $a \gtrsim 1.5$ AU with $\tau_{\rm deple}$ =1-10 Myr and $e_{\rm J} < 0.1$. The protoplanets beyond 2 AU are delivered to the terrestrial region. Inside of 2AU, the secular resonance promotes orbital crossings of oligarchs, but does not trap them. There, semimajor axis decay only happens as a result of (brief) eccentricity damping after collisions or scatterings. Therefore, the planetary accumulation inside of 2AU is similar to that of the standard model, other than the final small eccentricities and inclinations.

Fig. 8 shows histograms of the semimajor axes of the three largest and smaller planets in multiple realizations of the dynamical shakeup model, using the same standard parameters as in Fig. 6 . The largest planet typically ends up at 0.8–0.9 AU; the second largest planet lies close to this planet at either 0.5–0.7 AU or 1–1.2 AU. In their direct N-body calculations, *Kokubo et al.* (2006a) derived similar results. Smaller planets are distributed throughout 0.5–1.5 AU, with a preference of 1.3 AU, slightly inside the orbit of Mars. Although the model does not simulate the formation of the asteroid belt, migration of protoplanets might account for e and i of asteroids and the loss of primordial material from the asteroid belt.

Table 1 compares average orbital elements of these calculations with the orbits of the terrestrial planets. The model produces good analogs for Earth and Venus, but the Mars and Mercury analogs are more massive than their real counterparts despite the loss of $\sim 1\ M_\oplus$ swept through the inner edge (0.3 AU) of a typical simulation. Because the gas damps e for all planets, e and i are independent of mass. Thus, while the results for the Earth and Venus analogs are reasonably close to those in the Solar System, the derived e and i for Mercury and Mars are low. Investigating how these results depend on the initial conditions is a top priority for the next set of simulations.

Calculations with multiple damping efficiencies and $e_{\rm J}$ illustrate the sensitivity of the results on some of the initial conditions (Fig. 7). All models produce some planets with small e. However, strong damping yields more lower mass planets, which start to interact dynamically once the gas is depleted (see also *Iwasaki et al.*, 2001, 2002). Weak damping cases resemble calculations of chaotic growth. Because planets leftover after the gas disappears in the strong damping case will eventually form massive planets with eccentric orbits, the strong and weak damping limits tend to produce planets on eccentric orbits. The moderate damping cases have the best chance forming a few massive planets with fairly circular orbits.

5. CONCLUSION AND IMPLICATIONS

The numerical calculations summarized here have several interesting consequences for the evolution of terrestrial planets. The transition from oligarchic to chaotic growth and the final accretion phase finish on timescales, $\sim$ a few Myr to $\sim$ 80 Myr, before radiometric evidence suggests the formation of the Earth was fairly complete (*Yin et al.*, 2002). Planets are also fully formed well before the estimated time of the Late Heavy Bombardment, $\sim$ 100–600 Myr after the formation of the Sun (*Tera et al.*, 1974; *Ryder*, 2002; *Koeberl*, 2003).

Throughout the chaotic growth and cleanup phases, numerical calculations produce many lunar- to Mars-sized objects on highly eccentric orbits. These objects are good candidates for the 'giant impactor' that collided with the Earth to produce the Moon (*Hartmann and Davis*, 1975; *Cameron and Ward*, 1976; *Benz et al*, 1986; *Canup* 2004). As the numerical models become more complete, predicted mass and eccentricity distributions will yield better estimates for the probability of these events.

Historically, the Solar System provided the only test of models for planet formation. In the last decade, however,

TABLE 1
COMPARISON OF MODELS WITH THE SOLAR SYSTEM

Terrestrial planets					Model Results				
Planet	a(AU)	Mass ($M_\oplus$)	$\langle e \rangle$	$\langle i_{\rm inv} \rangle$ (rad)	Region (AU)	N	Mass ($M_\oplus$)	e	$i_{\rm inv}$ (rad)
Mercury	0.387	0.0553	0.16	0.12	0-0.5	14	0.68	0.042	0.038
Venus	0.723	0.815	0.031	0.026	0.5-0.85	36	0.80	0.037	0.045
Earth	1.00	1.00	0.028	0.021	0.85-1.25	39	0.86	0.036	0.031
Mars	1.52	0.107	0.19	0.073	>1.25	28	0.33	0.048	0.056

radial velocity surveys (*Udry et al.*, this volume) and transit observations (*Charbonneau et al.*, this volume) have detected over 150 extrasolar gas giants around nearby stars. Aside from *Kepler, http://www.kepler.arc.nasa.gov*, detections of terrestrial planets require advanced technology on new facilities. Here, we describe a few tests of debris disk simulations and some prospects for direct detections of terrestrial planets.

Direct detections of terrestrial planets require telescopes with large aperture and high spatial resolution. When terrestrial planets first form, they are probably molten, with effective temperatures $\sim$ 1500 K and relative luminosities $L_P/L_* \sim 10^{-7}$ to 10^{-6}. As terrestrial planets cool, their temperatures and luminosities fall to $T \sim$ 200–400 K and $L_P/L_* \sim 10^{-10}$. Thus, mid-IR observations can reveal planets around very young stars. Optical and near-IR images are necessary to detect older terrestrial planets.

Within the next 10–20 yr, new facilities will enable direct detections of terrestrial planets. The *Terrestrial Planet Finder, http://planetquest.jpl.nasa.gov/TPF/* aims to detect habitable worlds around nearby F, G, and K stars, with a projected launch date c. 2016. On the same timescale, large-ground based telescopes such as the Giant Magellan Telescope (GMT, http://www.gmto.org/) may yield similar results. Current techniques in adaptive optics allow detections of point sources with $L_P/L_* \lesssim 10^{-6}$ at 1.65 μm (*Codona and Angel*, 2004; *Codona*, 2004). Modest improvements in this technology allow direct detections of molten 'Earths'; more dramatic improvements may enable direct detections of cooler terrestrial planets.

Detecting debris from terrestrial planets is much easier. With maximum $L_{\rm debris}/L_* \sim 10 - 100$ at 24 μm, IR excess emission from the dusty leftovers of terrestrial planet formation is easily detected around stars with ages $\sim$ 1–10 Myr (Fig. 1). As planets disperse this debris, scattered light and thermal emission from dust is detectable with current technology for $\sim$ 100–300 Myr. For example, *Chen and Jura* (2001) and *Song et al.* (2005) report dust from massive asteroid belts around ζ Lep and BD+20°307, two stars with ages of 100–300 Myr.

Recent comparsions between theory and large samples of A-type and G-type stars are encouraging: the observations show the slow decline in 24 μm excess predicted by theory (*Dominik and Decin*, 2003; *Rieke et al.*, 2005; *Najita and Williams*, 2005). At each stellar age, however, the data appear to show a larger range in dust temperatures and luminosities than predicted by theory (*Najita and Williams*, 2005). These comparisons suggest that external perturbations and stochastic events modify the relatively smooth evolution of IR excess in Fig. 1.

Ground-based and satellite projects can test other results of debris disk simulations. The four year *Kepler* mission should detect 2–5 eclipses from the debris clouds produced by large binary collisions (*Kenyon and Bromley*, 2005). The ground-based projects *OGLE*, *PASS*, and *TRES* projects may also have the sensitivity to detect debris clouds (*Konacki et al.*, 2004; *Alonso et al.*, 2004; *Deeg et al.*, 2004; *Pont et al.*, 2004). As part of a much deeper all-sky survey, Pan-STARRS (http://pan-starrs.ifa.hawaii.edu/public/index.html) might also detect eclipses from debris clouds. To detect the unique signal from a large two body collision, these projects need to distinguish real events with diminishing depth and lengthening duration from spurious signals and from repetitive eclipses with constant depth and duration.

New observations and better numerical calculations promise a better understanding of debris disks and the late stages of terrestrial planet formation. Larger samples from Spitzer and ground-based telescopes will enable better statistical comparisons. New facilities such as ALMA and GMT will provide resolved observations of debris disks in the terrestrial zones of nearby stars, enabling probes of the masses and orbits of planets in addition to the structure of the debris. These data will challenge efforts to build more complete numerical simulations of debris disk formation and the late stages of planet formation.

Acknowledgments. The authors acknowledge J. Chambers for his helpful review. We also thank E. Kokubo for his kind data offering and M. Holman for useful discussions. MN is supported by MEXT under grant MEXT-16077202. EWT is supported by the Natural Sciences and Engineering Research Council of Canada, and by CITA. BCB and SJK acknowledge support from the NASA Astrophysics Theory Program (grant NAG5-13278) and supercomputing support from the JPL Institutional Computing and Information Services and the NASA Directorates of Aeronautics Research, Science, Exploration Systems, and Space Operations. This work was partially supported by NASA un-

der grant NAGS5-11779 and NNG04G-191G, by JPL under grant 1228184, and by NSF under grant AST-9987417 through DNCL.

REFERENCES

Abe Y., Ohtani E., Okuchi T., Righter K., and Drake M. (2000) In *Origin of the Earth and Moon* (R. M. Canup and K. Righter, eds.), Univ. of Arizona, Tucson, p. 413-433.

Adachi I., Hayashi C., and Nakazawa K. (1976) *Prog. Theor. Phys., 56*, 1756-1771.

Agnor C. B., Canup R. M., and Levison H. F. (1999) *Icarus, 142*, 219-237.

Agnor C. B. and Ward W. R. (2002) *Astrophys. J., 567*, 579-586.

Agnor C. and Asphaug E. (2004) *Astrophys. J., 613*, L157-L160.

Alonso R., Brown T., Torres G., Latham D. W., Sozzetti A. et al. (2004) *Astrophys. J., 613*, L153-L156.

Armitage P. J. (2003) *Astrophys. J., 582*, L47-L50.

Artymowicz P. (1993) *Astrophys. J., 419*, 166-180.

Balsiger H., Altwegg K., and Geiss J. (1995) *Jour. Geophys. Res., 100*, 5827-5834.

Barbieri M., Marzari F., and Scholl H. (2002) *Astron. Astrophys., 396*, 219-224.

Butler R. P., Marcy G. W., Fischer D. A., Brown T. M., Contos A. R. et al. (1999) *Aastrophys. J., 526*, 916-927.

Benz W. and Asphaug E. (1999) *Icarus, 142*, 5-20.

Benz W., Slattery W. L., and Cameron A. G. W. (1986) *Icarus, 66*, 515-535.

Bockelee-Morvan D., Gautier D., Lis D. C., Young K., Keene J. et al. (1998) *Icarus, 133*, 147-162.

Bromley B. C. and Kenyon S. J. (2006) *Astron. J.*, in press.

Cameron A. G. W. and Ward W. R. (1976) *Abst. Lunar Planetary Sci. Conf., 7*, 120-120.

Canup R. (2004) *Ann. Rev. Astron. Astrophys., 42*, 441-475.

Chambers J. E. (2001) *Icarus, 152*, 205-224.

Chambers J. E. and Cassen P. (2002) *Meteoritics & Planet. Sci., 37*, 1523-1540.

Chambers J. E. and Wetherill G. W. (1998) *Icarus, 136*, 304-327.

Chambers J. E., Wetherill G. W., and Boss A. P. (1996) *Icarus, 119*, 261-268.

Chen C. H. and Jura M. (2001) *Astrophys. J., 560*, L171-L174.

Codona J. L. (2004) *Proc. SPIE, 5490*, 379-388.

Codona J. L. and Angel R. (2004) *Astrophys. J., 604*, L117-L120.

Cox L. P. and Lewis J. S. (1980) *Icarus, 44*, 706-721.

Drake M. J. (2005) *Meteoritics & Planetary Science, 40*, 519-527.

Drake M. J. and Righter K. (2002) *Nature, 416*, 39-44.

Dauphas N., Robert F., and Marty B. (2000) *Icarus, 148*, 508-512.

Deeg H. J., Alonso R., Belmonte J. A., Alsubai K., Horne K. et al. (2004) *Publ. Astron. Soc. Pac., 116*, 985-995.

Dominik C. and Decin G. (2003) *Astrophys. J., 598*, 626-635.

Duncan M. J., Levison H. F., and Lee M. H. (1998) *Astron. J., 116*, 2067-2077.

Durda D. D., Greenberg R., and Jedicke R. (1998) *Icarus, 135*, 431-440.

Durda D. D., Bottke W. F., Enke B. L., Merline W. J., Asphaug E. et al. (2004) *Icarus, 170*, 243-257.

Fogg M. J. and Nelson R. P. (2005) *Astron. Astrophys., 441*, 791-806.

Goldreich P., Lithwick Y., and Sari R. (2004) *Ann. Rev. Astron. Astrophys., 42*, 549-601.

Goldreich P. and Tremaine S. (1980), *Astrophys. J., 241*, 425-441.

Goldreich P. and Ward W. R. (1973) *Astrophys. J., 183*, 1051-1062.

Gomes R., Levison H. F., Tsiganis K., and Morbidelli A. (2005) *Nature, 435*, 466-469

Greenberg R., Hartmann W. K., Chapman C. R., and Wacker J. F. (1978) *Icarus, 35*, 1-26.

Grogan K., Dermott S. F., and Durda D. D. (2001) *Icarus, 152*, 251-267.

Halliday A. N. (2004) *Nature, 427*, 505-590.

Halliday A. N., Lee D-C., and Jacobsen S. B. (2000) In *Origin of the Earth and Moon* (R. M. Canup and K. Righter, eds.), pp. 45-62. Univ. of Arizona, Tucson.

Hayashi C. (1981) *Prog. Theor. Phys. Suppl., 70*, 35-53.

Hayashi C., Nakazawa K., and Nakagawa Y. (1985) In *Protostars and planets II* (D. C. Black and M. S. Matthews, eds.), pp. 1100-1153. Univ. of Arizona, Tucson.

Hartmann W. K. and Davis D. R. (1975), *Icarus, 24*, 504-514.

Heppenheimer T. A. (1978) *Astron. Astrophys., 65*, 421-426.

Holsapple K. L (1994) *Planet. Space Sci., 42*, 1067-1078.

Housen K. and Holsapple K. (1990) *Icarus, 84*, 226-253.

Housen K. and Holsapple K. (1999) *Icarus, 142*, 21-33.

Ida S. and Makino J. (1993) *Icarus, 106*, 210-227. 875-889.

Inaba S., Tanaka H., Nakazawa K., Wetherill G. W., and Kokubo E. (2001) *Icarus, 149*, 235-250.

Ito T. and Tanikawa K. (1999) *Icarus, 139*, 336-349.

Iwasaki K., Tanaka H., Nakazawa K., and Emori H. (2001) *Publ. Astron. Soc. Japan, 53*, 321-329.

Iwasaki K., Emori H., Nakazawa K., and Tanaka H. (2002) *Publ. Astron. Soc. Japan, 54*, 471-479.

Jacobsen S. B. (2005) *Ann. Rev. Earth Planet. Sci., 33*, 531-570.

Jones B. W., Sleep P. N., and Chambers J. E. (2001) *Astronomy Astrophys., 366*, 254-262

Kenyon S. J. and Bromley B. C. (2002) *Astrophys. J., 577*, L35-L38.

Kenyon S. J. and Bromley B. C. (2004a) *Astron. J., 127*, 513-530.

Kenyon S. J. and Bromley B. C. (2004b) *Astrophys. J., 602*, L133-L136.

Kenyon S. J. and Bromley B. C. (2005) *Astron. J., 130*, 269-279.

Kenyon S. J. and Bromley B. C. (2006) *Astron. J., 131*, No. 3.

Kenyon S. J. and Hartmann L. W. (1995) *Astrophys. J. Suppl., 101*, 117-171.

Koeberl C. (2003) *Earth Moon Planets, 92*, 79-87.

Kokubo E. and Ida S. (1995) *Icarus, 114*, 247-257.

Kokubo E. and Ida S. (1996) *Icarus, 123*, 180-191.

Kokubo E. and Ida S. (1998) *Icarus, 131*, 171-178.

Kokubo E. and Ida S. (2000) *Icarus, 143*, 15-27.

Kokubo E. and Ida S. (2002) *Astrophys. J., 581*, 666-680.

Kokubo E., Kominami J., and Ida S. (2006a), *Astrophys. J.* accepted.

Kominami J. and Ida S. (2002) *Icarus, 157*, 43-56.

Kominami J. and Ida S. (2004) *Icarus, 167*, 231-243.

Konacki M., Torres G., Sasselov D. D., Pietrzyski G., Udalski A. et al. (2004) *Astrophys. J., 609*, L37-L40.

Kortenkamp S. J. and Wetherill G. W. (2000) *Icarus, 143*, 60-73.

Kortenkamp S. J., Kokubo E., and Weidenschilling S. J. (2000) In *Origin of the Earth and Moon* (R. M. Canup and K. Righter, eds.), pp. 75-84. Univ. of Arizona, Tucson.

Kortenkamp S. J., Wetherill G. W., and Inaba S. (2001) Science, 293, 1127-1129.

Laughlin G., Chambers J., and Fischer D. (2002) *Astrophys. J., 579*, 455-467.

Lecar M. and Aarseth S. J. (1986) *Astrophys. J., 305*, 564-579.

Levison H. F. and Agnor C. (2003) *Astron. J., 125*, 2692-2713.
Levison H. F., Dones L., Chapman C. R., Stern S. A., Duncan M. J., and Zahnle, K. (2001) *Icarus, 151*, 286-306.
Leinhardt Z. M. and Richardson D. C. (2005) *Astrophys. J., 625*, 427-440.
Lissauer J. J. (1987) *Icarus, 69*, 249-265.
Lissauer J. J. and Kary D. M. (1991) *Icarus, 94*, 126-159.
Lissauer J. J. and Stewart G. R. (1993) In *Protostars and Planets III* (E. H. Levy and J. J. Lunine, eds.), pp. 1061-1088. Univ. of Arizona, Tucson.
Lunine J. I., Chambers J., Morbidelli A., and Leshin L. A. (2003) *Icarus, 165*, 1-8.
Marcy G. W., Butler R. P., Fischer D. A., and Vogt S. S. (2004) In *Extrasolar Planets: Today and Tomorrow* (J. P. Beaulieu, E. A. Lecavelier, and C. Terquem, eds.), pp. 3-14. Astron. Soc. Pacific, San Francisco.
Marzari F. and Scholl, H. (2000) *Astrophys. J., 543*, 328-339.
Mayor M. and Queloz D. (1995) *Nature, 378*, 355-359.
Mayor M., Udry S., Naef D., Pepe F., Queloz D. et al. (2004) *Astron. Astrophys., 415*, 391-402.
McArthur B. E., Endl M., Cochran W. D., Benedict G. F., Fischer D. A. et al. (2004) *Astrophys. J., 614*, L81-L84.
McNeil D., Duncan M. J., and Levison H. F. (2005), *Astron J., 130*, 2884-2899.
Meier R., Owen T. C., Jewitt D, C., Matthews H. E., Senay M. et al. (1998) *Science, 279*, 1707-1710.
Michel P., Benz W., Tanga P., and Richardson D. C. (2001)*Science, 294*, 1696-1700.
Morbidelli A., Chambers J., Lunine J. I., Petit J. M., Robert F. et al. (2000) *Meteoritics & Planet. Sci., 35*, 1309-1320.
Nagasawa M., Tanaka H., and Ida S. (2000) *Astron. J., 119*, 1480-1497.
Nagasawa M., Lin D. N. C., and Thommes E. (2005) *Astrophys. J., 635*, 578-598.
Najita J. and Williams J. P. (2005) *Astrophys. J., 635*, 625-635.
Ohtsuki K., Ida S., Nakagawa Y., and Nakazawa K. (1993) In *Protostars and Planets III* (E. H. Levy and J. I. Lunine, eds.), pp. 1089-1107. Univ. of Arizona, Tucson.
Ohtsuki K., Stewart G. R., and Ida S. (2002) *Icarus, 155*, 436.
Pollack J. B., Hubickyj O., Bodenheimer P., Lissauer J. J., Podolak M. et al. (1996) *Icarus, 124*, 62-85.
Pont F., Bouchy F., Queloz D., Santos N. C., Melo C. et al. (2004) *Astron. Astrophys., 426*, L15-L18.
Quintana E. V., Lissauer J. J., Chambers J. E., and Duncan M. (2002) *Astrophys. J., 576*, 982-996.
Raymond S. N., Quinn T., and Lunine J. I. (2004) *Icarus, 168*, 1-17.
Raymond S. N., Quinn, T., and Lunine J. I. (2005a) *Astrophys. J., 632*, 670-676.
Raymond S. N., Quinn T,, and Lunine J. I. (2005b) *Icarus, 177*, 256-263.
Rieke G. H., Su K. Y. L., Stansberry J. A., Trilling D., Bryden G. et al. (2005) *Astrophys. J., 620*, 1010-1026.
Ryder G. (2002) *Journ. Geophys. Res., 107*, 6-26.
Safronov V. (1969) In *Evolution of the Protoplanetary Cloud and Formation of the Earth and Planets*, Nauka Press, Moscow.
Sasaki T. and Abe Y. (2005) In *PPV Poster Proceedings* http://www.lpi.usra.edu/meetings/ppv2005/pdf/8221.pdf
Song I., Zuckerman B., Weinberger A. J., and Becklin E. E. (2005) *Nature, 436*, 363-365.
Tanaka H. and Ida S. (1999) *Icarus, 139*, 350-366.
Tanaka H. and Ward W. R. (2004) *Astrophys. J., 602*, 388-395.
Tanaka H., Takeuchi T., and Ward W. R. (2002) *Astrophys. J., 565*, 1257-1274.
Tera F., Papanastassiou D. A., and Wasserburg G. J. (1974) *Earth Planet. Sci., 22*, L1-L21.
Thébault P., Marzari F., and Scholl H. (2002) *Astron. Astrophys., 384*, 594-602.
Ward W. R. (1973) *Science, 181*, 260-262.
Ward W. R. (1981) *Icarus, 47*, 234-264.
Ward W. R. (1986) *Icarus, 67*, 164-180.
Ward W. R. (1989) *Astrophys. J., 345*, L99-L102.
Ward W. R. (1993) *Icarus, 106*, 274-287.
Ward W. R. (2000) In *Origin of the Earth and Moon* (R. M. Canup and K. Righter, eds.), pp. 75-84. Univ. of Arizona, Tucson.
Ward, W. R., Colombo, G., and Franklin, F. A. (1976), Icarus, 28, 441-452.
Weidenschiling S. J. (1995) *Icarus, 116*, 433-435.
Weidenschilling S. J. and Cuzzi J. N. (1993) In *Protostars and Planets III* (E. H. Levy and J. J. Lunine, eds.), pp. 1031-1060. Univ. of Arizona, Tucson.
Weidenschilling, S. J., Spaute, D., Davis, D. R., Marzari, F., and Ohtsuki, K. (1997) *Icarus, 128*, 429-455.
Wetherill, G. W. (1980) *Ann. Rev. Astron. Astrophys., 18*, 77-113.
Wetherill G. W. (1985) *Science, 228*, 877-879.
Wetherill, G. W. (1990) *Icarus, 88*, 336-354.
Wetherill G. W. (1996) *Icarus, 119*, 219-238.
Wetherill G. W. and Stewart G. R. (1989) *Icarus, 77*, 330-357.
Wetherill G. W. and Stewart G. R. (1993) *Icarus, 106*, 190-209.
Wood B. J. and Halliday A. N. (2005) *Nature, 437*, 1345-1348.
Yin Q., Jacobsen S. B., Yamashita K., Blichert-Toft J., Telouk P. et al. (2002) *Nature, 418*, 949-952.
Youdin A. N. and Shu F. H (2002) *Astrophys. J., 580*, 494-505.
Zhou J.-L., Asrseth S. J., Lin D. N. C., and Nagasawa M. (2005) *Astrophys. J., 631*, L85-L88.